

1 **CO₂ and CH₄ exchanges between moist moss tundra and atmosphere on Kapp**
2 **Linne, Svalbard**

3 **Anders Lindroth¹, Norbert Pirk², Ingibjörg S Jónsdóttir³, Christian Stiegler⁴, Leif**
4 **Klemedtsson⁵, and Mats B Nilsson⁶**

5 ¹Department of Physical Geography and Ecosystem Science, Lund University, Lund, Sweden.

6 ²Department of Geosciences, University of Oslo, Oslo, Norway.

7 ³Life and Environmental Sciences, University of Iceland, Reykjavik, Iceland.

8 ⁴Bioclimatology, Georg-August Universität Göttingen, Göttingen, Germany.

9 ⁵Department of Earth Sciences, University of Gothenburg, Gothenburg, Sweden.

10 ⁶Department of Forest Ecology and Management, Swedish University of Agricultural Sciences,
11 Umeå, Sweden.

12 Corresponding author: anders.lindroth@nateko.lu.se

13 Abstract

14 We measured CO₂ and CH₄ fluxes using chambers and eddy covariance (only CO₂) from a moist
15 moss tundra in Svalbard. The average net ecosystem exchange (NEE) during the summer (9
16 June-31 August) was negative (sink) with $-0.139 \pm 0.032 \mu\text{mol m}^{-2}\text{s}^{-1}$ corresponding to -11.8 g C
17 m^{-2} for the whole summer. The cumulated NEE over the whole growing season (day no. 160 to
18 284) was -2.5 g C m^{-2} . The CH₄ flux during the summer period showed a large spatial and
19 temporal variability. The mean value of all 214 samples was $0.000511 \pm 0.000315 \mu\text{mol m}^{-2}\text{s}^{-1}$
20 which corresponds to a growing season estimate of 0.04 to $0.16 \text{ g CH}_4 \text{ m}^{-2}$. Thus, we find that
21 this moss tundra ecosystem is closely in balance with the atmosphere during growing season
22 when regarding exchanges of CO₂ and CH₄. The sink of CO₂ as well as the source of CH₄ are
23 small in comparison with other tundra ecosystems in high Arctic.

24
25 Air temperature, soil moisture and greenness index contributed significantly to explain the
26 variation in ecosystem respiration (R_{eco}) while active layer depth, soil moisture and greenness
27 index were the variables that best explained CH₄ emissions. Estimate of temperature sensitivity
28 of R_{eco} and gross primary productivity (GPP) showed that the sensitivity is slightly higher for
29 GPP than for R_{eco} in the interval $0 - 4.5 \text{ }^\circ\text{C}$, thereafter the difference is small up to about $6 \text{ }^\circ\text{C}$ and
30 then it began to raise rapidly for R_{eco} . The consequence of this, for a small increase in air
31 temperature of 1 degree (all other variables assumed unchanged) was that the respiration
32 increased more than photosynthesis turning the small sink into a small source (4.5 g C m^{-2}) during
33 the growing season. Thus, we cannot rule out that the reason why the moss tundra is close to
34 balance today is an effect of the warming that has already taken place in Svalbard.

35 1 Introduction

36 Climate warming is predicted to be most evident at high latitudes (Friedlingstein et al., 2006)
37 with profound effects on ecosystem functioning. One of the high latitude regions that are
38 expected to experience the most dramatic changes caused by climate change is the Arctic. This
39 region which is located roughly north of the tree-line is characterized by cold winters and cool
40 summers and with mean annual temperatures below zero. The summer periods are short ranging
41 between 3.5 to 1.5 months from the southern boundary to the north and July is normally the
42 warmest month. Annual precipitation is generally low decreasing from about 250 mm in the
43 southern areas to 45 mm in polar deserts in the north (Callaghan et al., 2005).

44
45 The permafrost soils in the Arctic store $1035 \pm 150 \text{ Pg}$ of organic carbon in the top 0-3 m
46 (Hugelius et al., 2014) which is more than the average 2010-2019 of 860 Pg of carbon in the
47 atmosphere (Friedlingstein et al., 2020). The increased warming in these areas can induce higher
48 decomposition rates due to increased microbial activity which will provide a positive feedback to
49 the climate system (Schuur et al., 2015). On the other hand, warming can also increase
50 photosynthesis and carbon uptake and thus compensate for, or exceed, the effect of increased
51 decomposition. Climate warming is also affecting plant community composition and the length
52 of the growing season (Post et al., 2009) which also has an impact on the processes regulating
53 annual carbon emissions and uptake (Bosiö et al., 2014). There is however a large uncertainty
54 regarding the timing, magnitude and possible sign of potential feedbacks caused by these
55 changes (Myers-Smith et al., 2020).

56

57 Understanding processes that are controlling the exchanges of greenhouse gases in the Arctic is
58 crucial for assessment of potential feedback effects. For this purpose, multiple year-around long-
59 term studies including direct measurements of CO₂ and CH₄ fluxes covering all seasons, winter,
60 spring, summer and autumn would be ideal. This is a great challenge in the harsh climate of the
61 Arctic and with limited support of key infrastructures for, e.g., provision of electricity for
62 operation of instruments.

63
64 In spite of these difficulties a few year-around studies have been performed during the last
65 couple of decades. In the low Arctic, Oechel et al. (2013) demonstrate the importance of the
66 wintertime fluxes in a tussock tundra ecosystem in Alaska. They found that the non-summer
67 season emitted more CO₂ than the corresponding uptake during the summer resulting in a net
68 source to the atmosphere of about 14 g C m⁻² on an annual basis. They also showed that the
69 shoulder seasons, spring and autumn roughly out-weighted the summer uptake. Euskirchen et al.
70 (2012, 2016) measured net CO₂ exchange in three different tundra ecosystems; heath tundra,
71 tussock tundra and wet sedge tundra in northern Alaska over three years. They found that the
72 uptake of -51 to -95 g C m⁻² during the summer (June-August) was overturned by the respiration
73 that occurred during the winter period resulting in net annual losses for all three ecosystems.
74 Zhang et al. (2019) reported five years of year-around flux measurements in a heath ecosystem
75 on west Greenland and they found that the heath was an annual sink of -35±15 g C m⁻². One year
76 with an anomalously deep snow pack showed a 3-fold higher respiration during the winter as
77 compared to the other years which resulted in a significantly lower net uptake during that year.

78
79 Even fewer studies have been done on year-around studies in the high Arctic. Lüers et al. (2014)
80 quantified the annual CO₂ budget using eddy covariance measurements in a river catchment area
81 near Ny-Ålesund on Spitsbergen in the Svalbard archipelago and they found that the ecosystem
82 was in C-balance. The footprint area was a semi-polar desert with only 60% vegetation cover and
83 patches of bare soil and stones. Also in Svalbard but further south in Adventdalen on a flat
84 alluvial fen irregularly covered with ice wedged polygons, Pirk et al. (2017) made year-around
85 measurements of CO₂ fluxes and found it to be a net sink of -82 g C m⁻². Because of the
86 irregularities caused by the ice wedges and the differences in wetness, they focused the analyses
87 on the spatial variability in two different directions, one wetter and one drier, and they estimated
88 the annual net ecosystem exchange to -91 g C m⁻² and -62 g C m⁻² for the respective areas.

89
90 The Arctic ecosystems constitute also a source of CH₄ to the atmosphere even if it is not a very
91 large one. Saunois et al. (2020) estimated that the Northern high latitude region (60°N - 90°N)
92 contributed 4% of global emissions and emissions from wetlands are only part of the emissions
93 from this region. However, in the light of the vulnerability of the high Arctic permafrost areas
94 and considering the large carbon pool and the predicted changes in climate, a quantification and
95 understanding of CH₄ exchanges in these areas are still important. Christensen et al. (2004)
96 showed one example of a dramatic impact of the climate warming on the CH₄ emissions in a
97 permafrost mire in sub-arctic Sweden. The warming which is visible in this area since decades
98 and its impact on permafrost and vegetation changes was estimated to have caused an increase of
99 landscape CH₄ emissions in the range 22-66% in the period 1970 to 2000.

100
101 Mastepanov et al. (2008) were the first to show the importance of emissions also outside of the
102 growing season. They observed a large burst of CH₄ from a fen area in Zackenberg, Greenland

103 after the growing season and during the time when the soil started to freeze. This finding was
104 confirmed in a later paper (Mastepanov et al., 2013) and the process was hypothetically
105 attributed to the subsurface CH₄ pool. Hydrology and vegetation composition play an important
106 role for CH₄ emission and dynamics. McGuire et al. (2012) made a comprehensive summary of
107 CH₄ exchanges of the Arctic tundra showing the difference between wet and dry ecosystems; the
108 wet tundra emitted 5.4 to 13.0 g CH₄-C m⁻² during summer and 8.5 to 20.2 g CH₄-C m⁻²
109 annually. The corresponding values for the dry/mesic tundra were 0.3 to 1.4 g CH₄-C m⁻² and 0.3
110 to 4.3 g CH₄-C m⁻², respectively. Bao et al. (2021) utilized year-around measurements of CH₄
111 fluxes from three sites of the Ameriflux network in Northern Alaska to demonstrate the
112 importance of the spring and autumn seasons for the annual emission. The shoulder seasons
113 contributed about 25% of the annual emissions and the autumn season had about three times
114 higher emission than the spring season. These findings increasingly emphasise the importance of
115 year-around measurements to fully understand the CH₄ controls and dynamics.
116

117 The main aim of this study is to provide another piece of the puzzle concerning CO₂ and CH₄
118 exchanges from different but widespread ecosystem types in the high Arctic. We hypothesise
119 that this moist tundra ecosystem is a net carbon sink during the growing season and that the
120 summer emissions of methane will be at levels comparable with other methane emitting high
121 Arctic ecosystems. We made flux measurements of CO₂ and CH₄ in an moist moss tundra
122 ecosystem situated at Kapp Linne on the west coast of the Svalbard archipelago in 2015 and with
123 an additional campaign in 2016. The measurements in 2015 were done using both eddy
124 covariance system (CO₂) and chambers (CO₂ and CH₄) but only chambers in 2016. We quantify
125 ecosystem respiration (R_{eco}), gross primary productivity (GPP) and net ecosystem exchange
126 (NEE) during the growing season based on a combination of chamber end eddy covariance
127 measurements. The CH₄ emission was only quantified for the summer season. We also analyze
128 the environmental controls of the fluxes.

129 **2 Materials and Methods**

130 **2.1 Research site and measurements**

131
132 This study was performed in the Svalbard archipelago near the weather station Isfjord Radio
133 (78°03'08" N 13°36'04" E, alt. 7 m) which is located right on the foreland of Kapp Linné on the
134 island of Spitzbergen (Fig. S1). The tundra area where the measurements were performed is
135 located about 1 km southeast of the station. The study area consists of moist moss tundra, a
136 widespread ecosystem in Svalbard (Vanderpuye et al., 2002; Ravolainen et al., 2020). The
137 vegetation is characterised by the moss species *Tomentypnum nitens*, *Sanionia uncinata* and
138 *Aulacomium palustre* and a sparse cover of vascular plants (20-40%), dominated by *Equisetum*
139 *arvense*, *Salix polaris* and *Bistorta vivipara*. Other vascular plant species found in the plots:
140 *Saxifraga cespitosa*, *Saxifraga oppositifolia*, *Silene aucaulis*, and some grass species, most likely
141 *Alopecurus ovatus* (previously *A. borealis*), and *Poa arctica*. The vegetation analysis was made
142 from photographs of chamber location plots taken between 26 June and 2 July 2015 (see Figs.
143 S4a-4y in Supplement).
144

145 The net ecosystem exchange of CO₂ was measured with an eddy covariance (EC) system located
146 centrally on the moss tundra (78°03'28.6" N 13°38'40" E). The sonic anemometer (USA-1;

147 Metek GmbH, Germany) was mounted on top of a tripod (see Fig. S1) at 2.7 m height. The CO₂
148 and H₂O concentrations were measured with an open path sensor (LI-7500; Li-Cor Inc., USA)
149 placed just beneath the sonic and inclined about 30° pointing towards east. Radiation
150 components, incoming and outgoing short-wave and long-wave (CNR-4; Kipp & Zonen, the
151 Netherlands) were measured at 2.0 m height above ground with the sensor directed towards
152 south. All sensors were connected to a datalogger (CR-1000; Campbell Scientific, USA) which
153 was powered by a solar panel and a battery. The EC sensors were sampled and stored at 10 Hz
154 and all other sensors were sampled at 0.1 Hz with storage of 30 min mean values. These
155 measurements were made from 25 June to 17 September 2015. The total data coverage during
156 this period was 47% with a longer break in the measurements between 28 July and 29 August.
157 The impact of substantial gap filling of measured EC data and partial modelling in order to
158 complete the full growing season is further discussed below.

159
160 The soil efflux of CO₂ and CH₄ was measured with a dark chamber connected to a gas analyzer
161 (Ultraportable Greenhouse Gas Analyzer; Los Gatos Research, USA) on 24 locations within the
162 EC average footprint area. A circular thin-steel frame, 15 cm in diameter and 15 cm high, was
163 inserted ca 5 cm into the ground in each location. The sharp edge of the frames made it easy to
164 insert them into the ground without damaging the vegetation and with minimal soil disturbance.
165 A picture was taken of each frame (see Supplement) for documentation of vegetation and for
166 calculation of different indexes. The chamber was also made from steel and it had a rubber seal
167 in the end facing the frame (Fig. S2) to make it air tight when mounted on the frame. The volume
168 of the chamber and the part of the frame raised above the surface was 5.3 L. A small fan was
169 installed inside the chamber to provide good mixing of the air during measurement. A small
170 weight (stone) was placed on top of the chamber during measurement to prevent it from moving
171 due to wind gusts. During concentration measurement air was circulated in a closed loop
172 between the chamber and the gas analyzer in ca. 10 m long 4 mm diameter polyethene tubes (see
173 Fig. S2). The air flow through the analyzer was ca 1.2 L min⁻¹. The chamber was ventilated in
174 the free air about 1 minute before each measurement which lasted for 5 minutes. The
175 concentrations were recorded and stored once per second by the gas analyzer. The time stamp of
176 the recorded data was used to identify measurement cycles for analysis of fluxes.

177
178 The chamber measurement positions were selected in the following way. The frames were
179 grouped in two sections, one north-east and one south-west of the flux tower since it was
180 expected that the main wind direction would be along that direction. Each group was then split
181 into three subsections with four measurement points within each one of them. The locations were
182 named S1:1-S1:4, S2:1-S2:4, S3:1-S3:4, N1:1-N1:4, N2:1-N2:4 and N3:1-SN3:4. The four
183 measurement points within each subsection were then placed along a transect with 3-4 m
184 between each point. This way it was possible to measure all four chamber locations without
185 having to move the whole measurement system. Chamber measurements were made in three
186 separate campaigns: mid-summer (26 June to 2 July 2015), late-summer (25-27 August 2015)
187 and early-summer (14-15 June 2016). Each location was measured three times during each one
188 of the three campaigns, a total of 216 measurements. Besides gas concentrations, also soil
189 temperature (5 cm), soil moisture (0-5 cm) and active layer depth was measured during each
190 campaign.

191

192 Meteorological data needed for analyses and gap-filling were obtained as follows: Hourly air
193 temperature and relative humidity from Isfjord radio, half-hourly global radiation from
194 Adventdalen, daily snow depth and ground ice conditions from Svalbard airport and monthly
195 precipitation from Isfjord radio and Barentsburg. The distance between the measurement site and
196 these stations are; Isfjord radio, 1 km, Barentsburg, 13 km, Svalbard airport, 46 km and
197 Adventdalen, 50 km. Using data from the more distant locations, Svalbard airport and
198 Adventdalen, introduces some additional uncertainty. Concerning global radiation data we could
199 compare in situ measured half-hourly radiation with the corresponding data from Adventdalen
200 for a shorter period and it showed general good agreement although with relatively large scatter
201 ($y = 0.84x + 15.9$; $r^2=0.57$; $n=580$). According to Dobler et al. (2021) the amount of precipitation
202 in the area where Kapp Linne and Svalbard airport are located don't show any significant
203 differences on an annual basis. Vickers et al. (2020) analysed timing of snow cover in Svalbard
204 and they show that the mean (2000-2019) first snow-free day is very similar in areas where Kapp
205 Linne and Svalbard airport are located. Thus, we are confident that using data from these
206 relatively remote locations does not introduce serious bias in our analyses. Data sources are
207 given in Acknowledgement.

208

209 **3. Data analysis**

210

211 The rawdata from the eddy covariance flux measurements were analysed using the Eddypro
212 software version 6.1.0 (Li-Cor, 2016). Correction was made for the impact of the additional heat
213 flux in the sensor path of the open path analyzer on the flux calculations according Burba et al.
214 (2008). Gap filling during the measurement period was made using the REdyProc online eddy
215 covariance data processing tool developed at the Max Planck Institute for Biogeochemistry
216 (Wutzler et al., 2018) without u^* correction since we could not identify any threshold for u^* . The
217 u^* threshold is generally low for low and smooth vegetation (Pastorello et al., 2020) and for a
218 wind exposed site as ours, it is not surprising that such threshold could not be found. Flux
219 partitioning was made with the daytime-based method according Lasslop et al. (2000). Only data
220 of highest quality, i.e. class=0 was retained for the gap filling and further analyses. Gap filling
221 outside of the EC measurement period to obtain the carbon balance for a full growing season was
222 made by modeling using the Lloyd & Taylor (1994) model for R_{eco} and an empirical light
223 response function for GPP (see below). The measured respiration by chambers was used to
224 obtain the parameters for R_{eco} and EC data was used for fitting of the light response function for
225 GPP.

226

227 For flux footprint calculations the roughness length (z_0) is needed and it was calculated from the
228 wind profile relationship in near neutral ($-0.01 < z/L < 0.01$) conditions:

229

$$230 \quad z_0 = \frac{z_m}{e^{\left(\frac{u(z)-k}{u^*}\right)}} \quad (1)$$

231

232 where z_m is measurement height, $u(z)$ is wind speed at height z , k is von Karman's constant and
233 u^* is friction velocity. We used the flux footprint prediction (FFP) online tool by Kjun et al.
234 (2015) to calculate the footprint climatology.

235

236 The fluxes from the chamber measurements were estimated from the time change of the
237 concentrations using linear regression. Every individual measurement was inspected and

238 evaluated manually. These inspections showed that 50 seconds for CO₂ and 100 seconds for CH₄
 239 were optimal to obtain near perfectly linear responses a few seconds after the chamber had been
 240 placed on the frame. The slopes of the regressions were then used to calculate fluxes per unit
 241 surface area. The flux detection limits for CO₂ and CH₄ were calculated in the following way:
 242 first the peak-to-peak variation in the respective gases were determined when the chamber was
 243 ventilated in the free air and when conditions were steady. Then 20 sets of artificial ‘fluxes’ for
 244 each gas species were estimated based on 100 randomly generated concentrations for each data
 245 set. The peak-to-peak difference was used as seed (input) for the randomly generated values. The
 246 95% value of the distribution of these randomly generated fluxes was taken as the flux detection
 247 limit for the respective gas.

249 The pictures of the vegetation inside of the chamber frames were analysed using the ImageJ
 250 (<https://imagej.net>) public domain software. The camera color channel information (digital
 251 numbers for Red (R), Green (G) and Blue (B) channels) was collected from the JPEG pictures.
 252 This type of pictures is for instance used in studies that are tracking the phenological
 253 development of vegetation (e.g. Richardson et al., 2009). The so-called green index (GI) is
 254 applied to detect differences in greenness of vegetation:

$$256 \quad GI = G/(R+G+B) \quad (2)$$

258 This index was also estimated for the central footprint area (100 m radius) of the flux
 259 measurement location using a picture taken at 160 m above the altitude of the measurement area.

260 Forward stepwise linear regression (Sigmaplot 12.5) was used to analyze the dependency of the
 261 CO₂ and CH₄ fluxes on environmental variables. We tested for air temperature (T_a), soil moisture
 262 (θ), soil temperature (T_s), active layer depth (ALD), measurement location (S_{id}) and GI.

264 For gap filling of R_{eco} we only had access to air temperature with full annual coverage and, thus,
 265 we could only use this driver for estimation of the R_{eco}. The measured chamber CO₂ fluxes were
 266 fitted to the Lloyd & Taylor (1994) model with air temperature (T_a) as independent variable:

$$268 \quad FCO_2 = a \cdot e^{b \left(\frac{1}{56.02} - \frac{1}{T_a + 46.02} \right)} \quad (3)$$

270 During the EC measurement period (25 June to 17 September 2015) the GPP was estimated as:

$$272 \quad GPP = NEE_f - R_{eco} \quad (4)$$

274 Where NEE_f is the gap filled NEE according to Wutzler et al. (2018). This way R_{eco} and GPP
 275 become consistent with the measured and gap filled NEE. For the time before and after this
 276 period NEE was estimated as the sum of modelled R_{eco} and modelled GPP. The data for the GPP
 277 model was derived from:

$$279 \quad GPP_m = NEE_m - R_{eco} \quad (5)$$

281 Where NEE_m is the measured net ecosystem exchange. The GPP_m was then fitted to a light
 282 response function:

283
284
$$GPP_m = c1 + c2 \cdot c3 / (c2 + R_g) \quad (6)$$

285

286 **4 Results**

287 For CO₂ exchanges and partitioning we combined the soil efflux measurements with the chamber
288 system with the eddy covariance flux measurements. This was crucial for the partitioning and for
289 gap filling because from 20 April to 20 August at this location the sun is above the horizon 24
290 hours of the day and this means that there were few occasions of dark nighttime measurements
291 with the eddy covariance system and all of these were collected at the very end of the summer.
292 We consider the chamber measurements that were distributed across the summer to be more
293 representative of R_{eco} for this location.

294

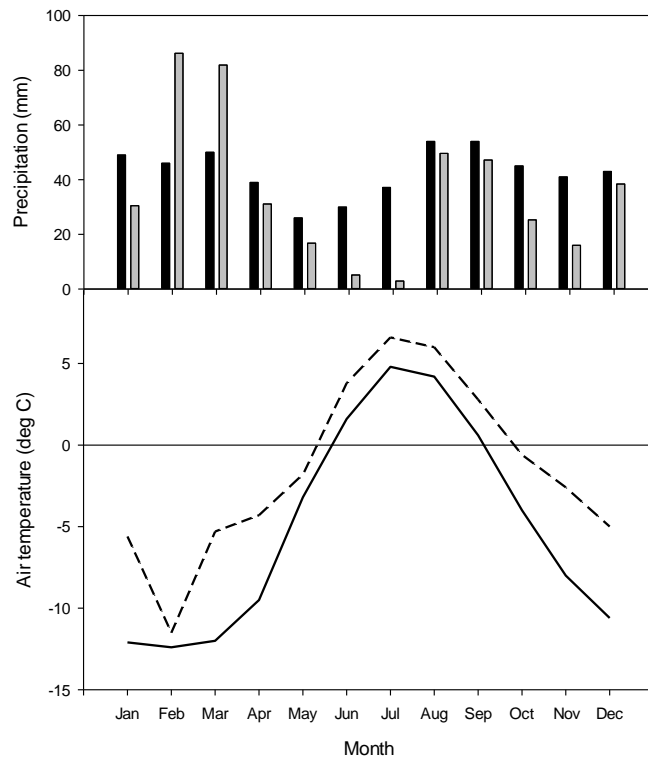
295 For CH₄ exchanges we don't have any eddy covariance measurements so we present only
296 chamber data for this variable.

297

298 **4.1 Weather**

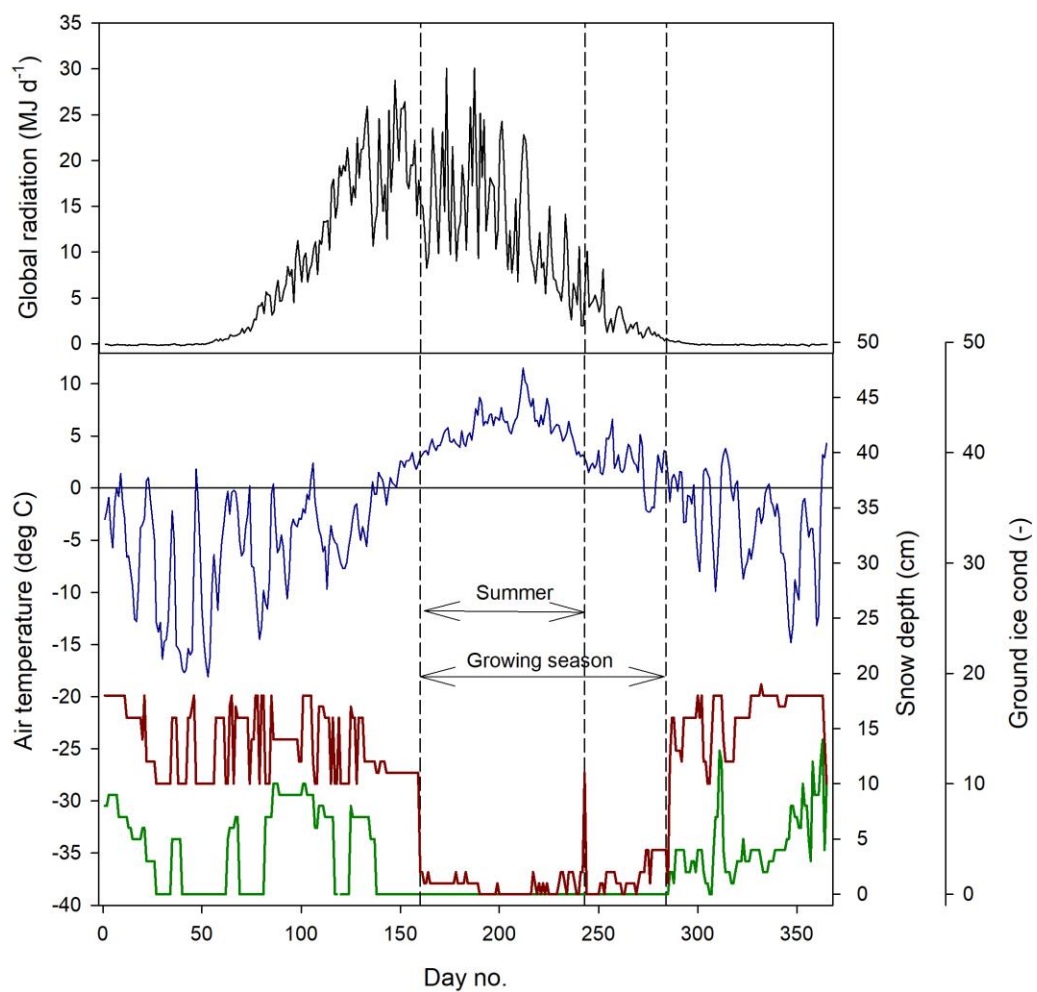
299

300 The mean annual temperature at Kapp Linne was -1.5 °C during 2015 which was 3.5 °C higher
301 than the long-term mean (1961-1990) of -5.1 °C. The summer (June-August) mean of 5.5 °C was
302 2.0 °C higher than the long-term mean for the same time period (Fig. 1). The summer
303 precipitation in 2015 was much lower, 58 mm as compared to the long-term precipitation which
304 was 121 mm. The annual precipitation was also lower, 431 mm compared to the long-term
305 precipitation which was 514 mm.



306
 307 Figure 1. Monthly precipitation (top): Long-term average 1961-1990 black bars and 2015 grey
 308 bars. Data from Barentsburg for January-May, from Isfjord Radio for June-December. Mean
 309 monthly air temperature (bottom): Solid line is long-term average 1961-1990 and dotted line is
 310 2015. Data from Isfjord Radio which is located about 1 km west of the investigation area.

311
 312 We defined the growing season (the period during which vegetation is photosynthesizing) based
 313 on the permanence of the snow pack which resulted in start day no. 160 and end day no. 284
 314 (Fig. 2). The summer period which normally is defined as June through August was here defined
 315 as lasting between 9 June (same as start of growing season) until end of August (Fig.2).
 316



317
 318
 319
 320

Fig. 2 Weather conditions during 2015. Top panel: Mean daily global radiation at Adventdalen. Bottom panel: Mean daily air temperature at Isfjord Radio (blue), snow depth (red) and ground

321 ice conditions (green) at Svalbard airport close to Longyearbyen. The ground ice condition is
322 scaled from 0 to 20 where 0 is no snow or ice on the ground and 20 indicate a complete cover of
323 snow or ice.

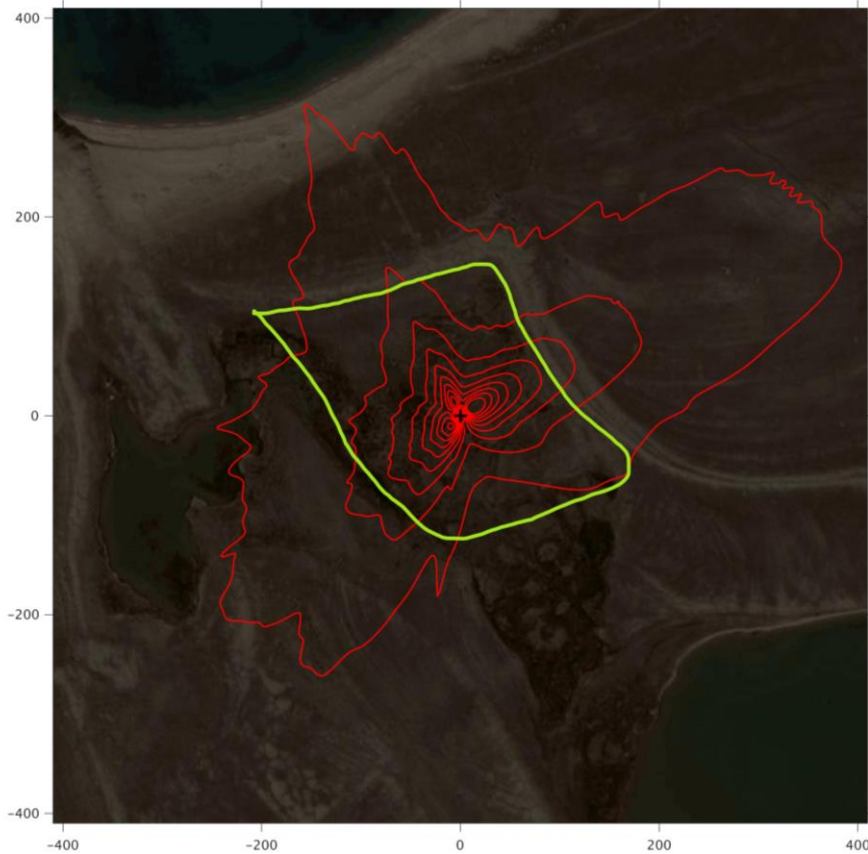
324

325 4.2 Flux footprint and greenness

326

327 The footprint climatology shows a good representativity of the moss tundra surface by the EC
328 measurements with 60-70% of fluxes emanating from areas well within the border of the tundra
329 (Fig. 3). The mean green index for a circular area with radius of 100 m centered at the flux tower
330 was 0.34 which corresponded exactly to the mean value for all chamber locations. The GI for the
331 24 chamber locations varied between 0.316 and 0.369. We observed a good (visual) correlation
332 between GI and coverage of green plants (see Figures S4a-S4y of chamber location pictures and
333 GI).

334



335

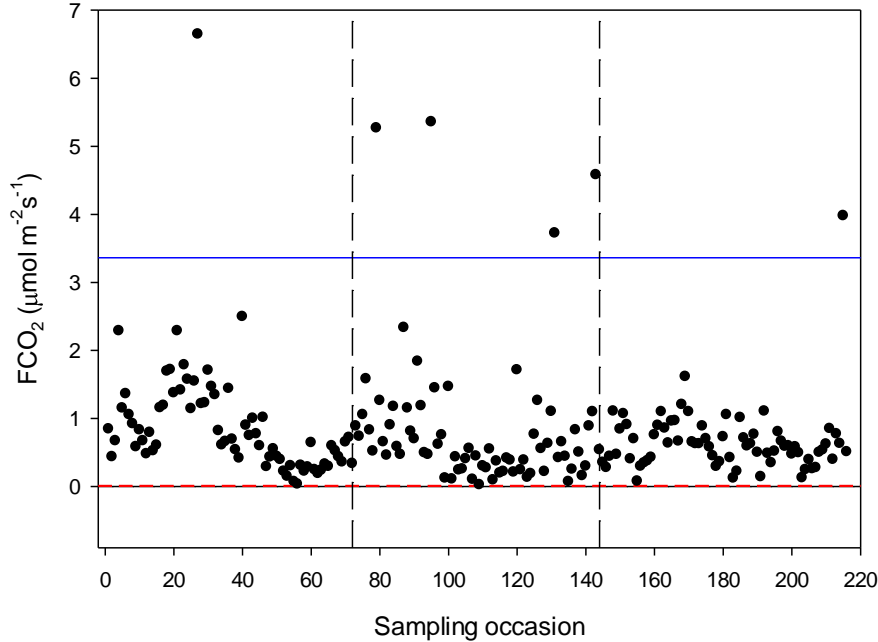
336 Figure 3. The footprint climatology with red contour lines 10-90%. The area within the green
337 line mark the heart of the moss tundra. The scale (m) is shown on the outer borders of the
338 picture.

339

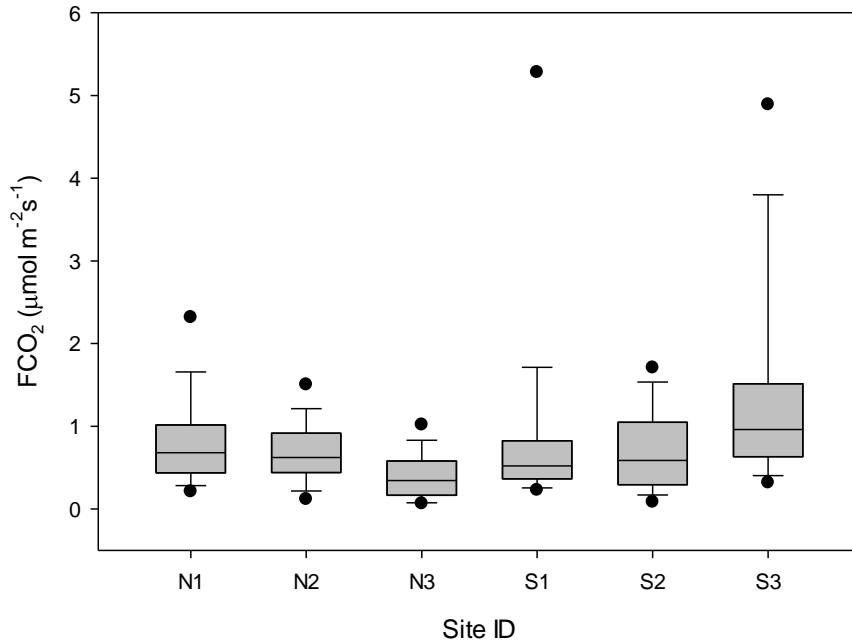
340 4.3 CO₂ exchanges

341

342 The CO₂ fluxes from the chamber measurements showed quite large variation over time (Fig. 4)
343 and across sampling locations (Fig. 5). The mean CO₂ flux of all samples was $0.81 \pm 0.11 \mu\text{mol}$
344 $\text{m}^{-2}\text{s}^{-1}$. The uncertainty is given as the 95 confidence limit.
345



346
347 Figure 4. Measured CO₂ exchange (FCO₂) from the 24 sampling points using dark chamber and
348 portable gas analyzer. The dashed red line indicates CO₂ flux detection limit and the blue line
349 represents 3xS.D. of all data points. The dashed vertical lines separate sampling periods from left
350 to right: 14-15 June, 26 June – 2 July and 25-27 August, respectively.



351

352 Figure 5. Box plot of CO₂ fluxes (FCO₂) per sampling location named N1-N3, S1-S3. The
 353 boundaries of the grey boxes represent the 25% and 75% percentiles, the line represent the
 354 median, whiskers above and below the boxes indicate the 10% and 90% percentiles. Outlying
 355 points are also shown.

356

357 Of the tested environmental variables T_a, θ, T_s, ALD, S_{id} and GI it was only T_a, θ and GI that
 358 contributed positively and significantly in decreasing order to explain the variability of the CO₂
 359 flux (Table 1).

360

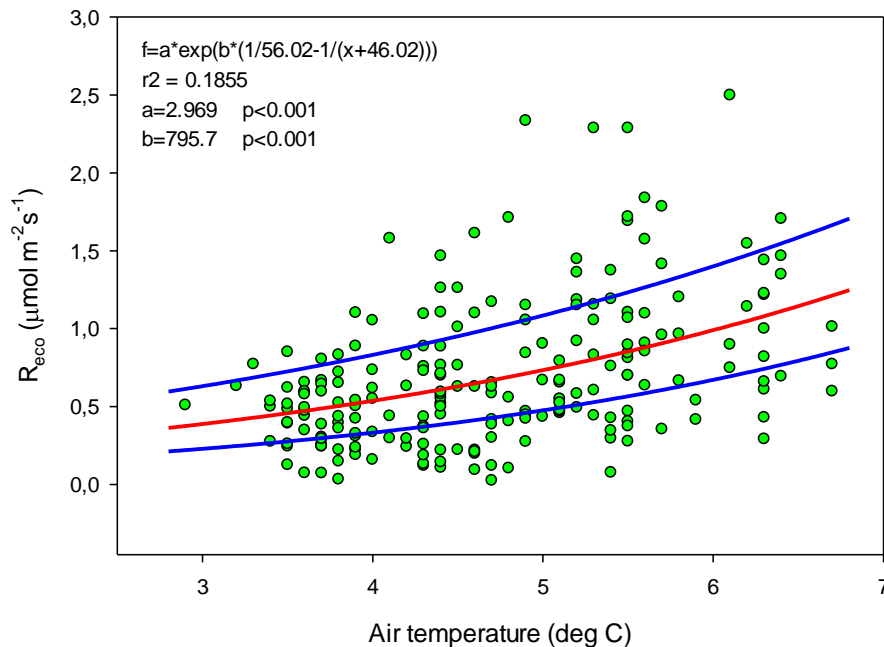
361 Table 1. Result of stepwise linear regression with CO₂ flux as dependent variable. Normality test
 362 failed but significance in all variables was confirmed with Wilcoxon Signed rank tests. T_a is air
 363 temperature, θ is soil moisture and GI is green index.

364

Variable	Partial-R ²	Probability (p)
T _a	0.190	<0.001
θ	0.037	0.002
GI	0.023	0.002

365

366 Ideally all of these variables should be used in a model to estimate R_{eco} for gap filling purposes
 367 but we could only use air temperature since this was the only variable that we had access to with
 368 complete coverage for a full year. The Lloyd & Taylor model (Eq. 3 & Fig. 6)) was thus used to
 369 estimate ecosystem respiration for 2015 using half-hourly air temperature as input.

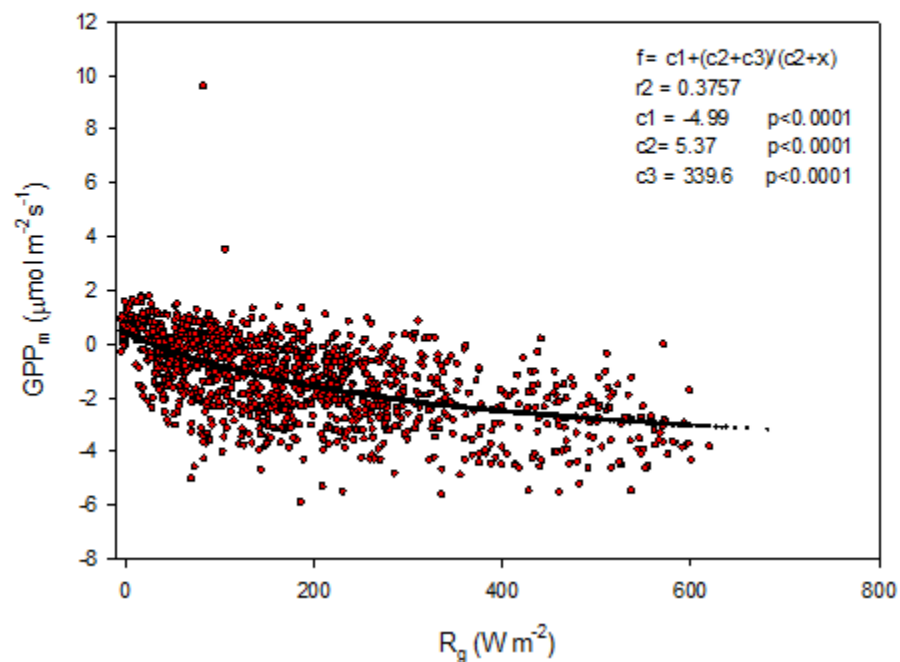


370

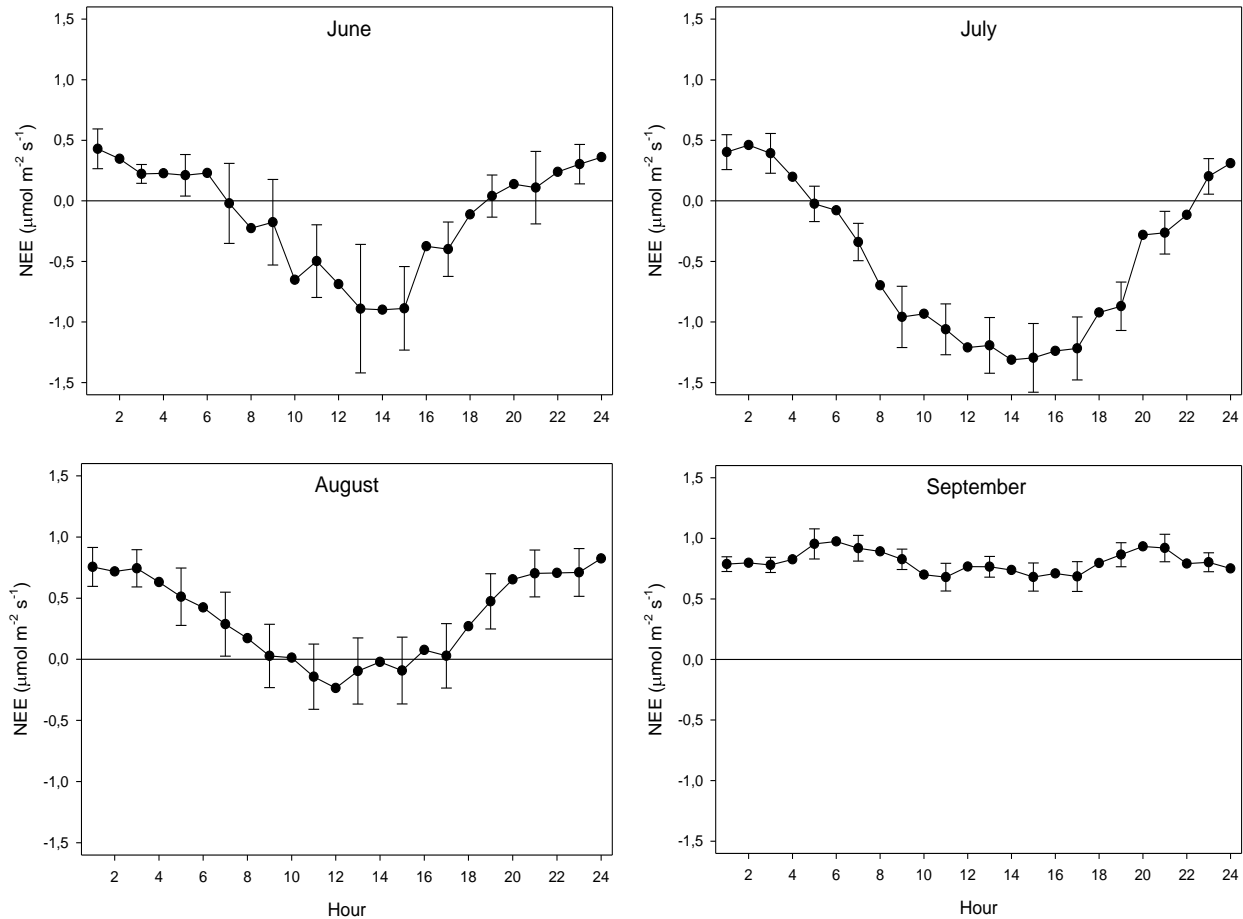
371 Figure 6. Measured ecosystem respiration (R_{eco}; green dots) using chambers plotted against air
 372 temperature. The red curve is the fitted equation and the blue curves are the corresponding
 373 boundaries when considering the standard deviation of the parameters.

374

375 The modelled gross primary productivity (Eq. 6; GPP_m) had a small offset when global radiation
376 was zero (Fig. 7). This offset was adjusted for when the model was applied for gapfilling so that
377 GPP become zero during nighttime.



378
379
380 Figure 7. Gross primary productivity (GPP_m) plotted against global radiation (R_g) ; red symbols
381 are estimated values according to eq. (5) and the black symbols are the fitted model.
382
383
384
385
386

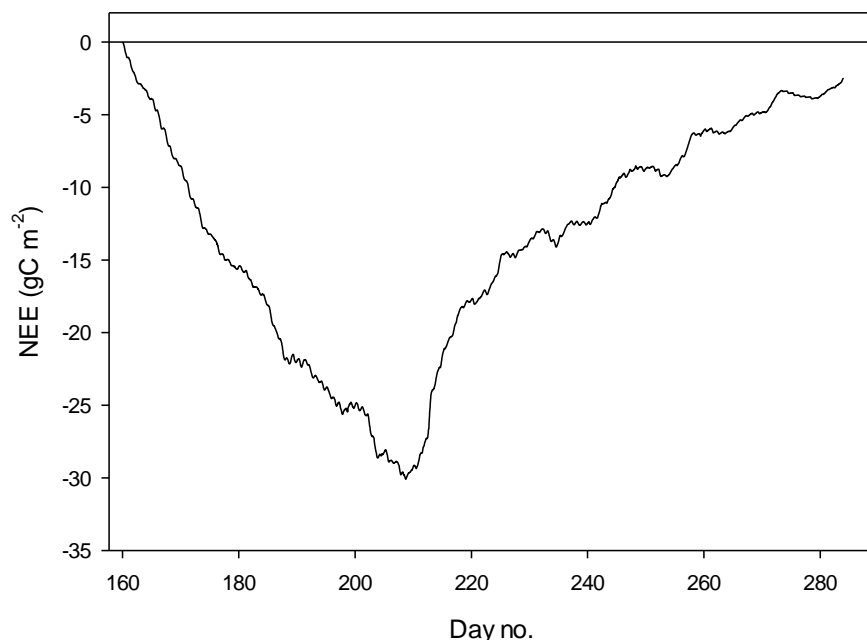


387
 388 Figure 8. The mean monthly diurnal course of net ecosystem exchange (NEE) during the period
 389 of eddy covariance measurements 25 June to 17 September. The error bars (every 2nd shown) are
 390 the 95% confidence interval. Notice that the main part of August was gap filled because of
 391 measurement problems.

392
 393
 394 The diurnal course of NEE during June - August exhibit the normal pattern with a successively
 395 increasing drawdown of CO₂ during first half of the day resulting in a maximum around noon. It
 396 should be noted that during June until 20 August the sun was over the horizon 24 hours, thus no
 397 dark period. The positive values at the beginning and end of the diurnal courses are a result of
 398 R_{eco} being larger than GPP. As pointed out in Fig. 8, most of the data of August were gapfilled
 399 causing some additional uncertainty. However, the diurnal course seems reasonable although the
 400 peak during noon is much lower as compared to July. This can be explained by the much lower
 401 incoming radiation in August as compared to July; the mean global radiation in July was 192 W
 402 m⁻² and 98 W m⁻² in August. The mean air temperature was similar during July and August. In
 403 September the incoming radiation is very low and thus GPP is also very low which result in a
 404 NEE that is dominated by the R_{eco} . The positive NEE values around mid-night during June –
 405 September are in good accordance with the values from the independent dark chamber
 406 measurements (Fig. 5).

407

408 In order to assess the impact of the large gap in measured data in August where we only had two
 409 days of measured fluxes at the end of the month we made a comparison between the gap filled
 410 diurnal course based on Wutzler et al. (2018) respectively our modelling using Eqs. 3 & 6. The
 411 results show very good agreement between the two methods (see Supplement) giving support to
 412 the realism and reliability of the gap filled data.
 413



414
 415 Figure 9. The cumulated half-hourly net ecosystem exchange (NEE) during growing season.
 416

417 The mean net CO₂ flux during the growing season was $-0.019 \pm 0.024 \mu\text{mol m}^{-2}\text{s}^{-1}$ with
 418 uncertainty given as the 95% confidence limit. The cumulated NEE during growing season
 419 ended up negative with -2.5 g C m^{-2} (Fig. 9). The mean net CO₂ flux during summer was $-$
 420 $0.139 \pm 0.032 \mu\text{mol m}^{-2}\text{s}^{-1}$ (95% confidence limit) and the cumulated NEE was -11.8 g C m^{-2}
 421 (Table 2).
 422

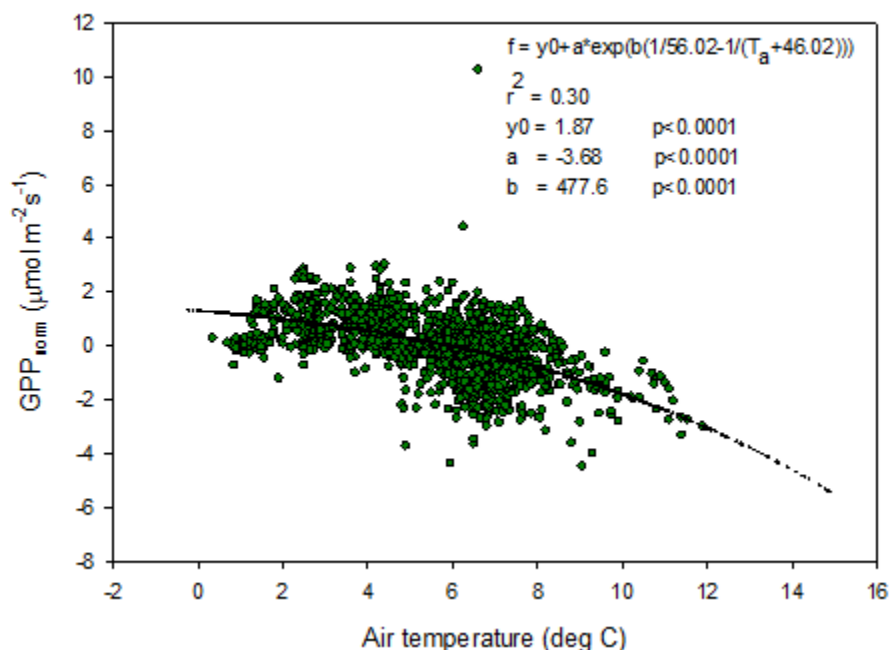
423 Table 2. Summary of seasonal C-fluxes from Kapp Linne. R_{eco} is ecosystem respiration, GPP is
 424 gross primary productivity and NEE is net ecosystem exchange.
 425

Period	Component	Value (gC m ⁻²)
Growing season	Reco	110.2
	GPP	-112.7
	NEE	-2.5
Summer	Reco	94.1
	GPP	-105.9
	NEE	-11.8

426
 427 4.4 Temperature sensitivity of R_{eco} and GPP

428

429 The temperature sensitivity of the R_{eco} is already given by the fitted Lloyd & Taylor (1994)
430 equation. In the absence of long time series of measurements during multiple year were natural
431 climate variability could be used to assess temperature sensitivity of GPP we approached this
432 problem in the following way. We normalize GPP for its dependence on radiation by estimating
433 the difference between the ‘measured’ GPP and the model which only depends on radiation (see
434 Fig. 7). A stepwise linear regression with normalized GPP as dependent variable and air
435 temperature, time of season and vapour pressure deficit as independent variables, showed that of
436 the total explained variance, air temperature stood for 94% and time of season and and vapour
437 pressure deficit for 3% each. Thus, the resulting normalized GPP show effectively a dependence
438 on air temperature (Fig. 10) with values becoming more negative, i.e. showing increasing GPP
439 with increasing temperature. We fitted the same type of model to these data as for the R_{eco} to be
440 able to compare sensitivities to temperature.



441

442 Figure 10. Normalized gross primary productivity (GPP) plotted against air temperature and with
443 the fitted exponential model.

444

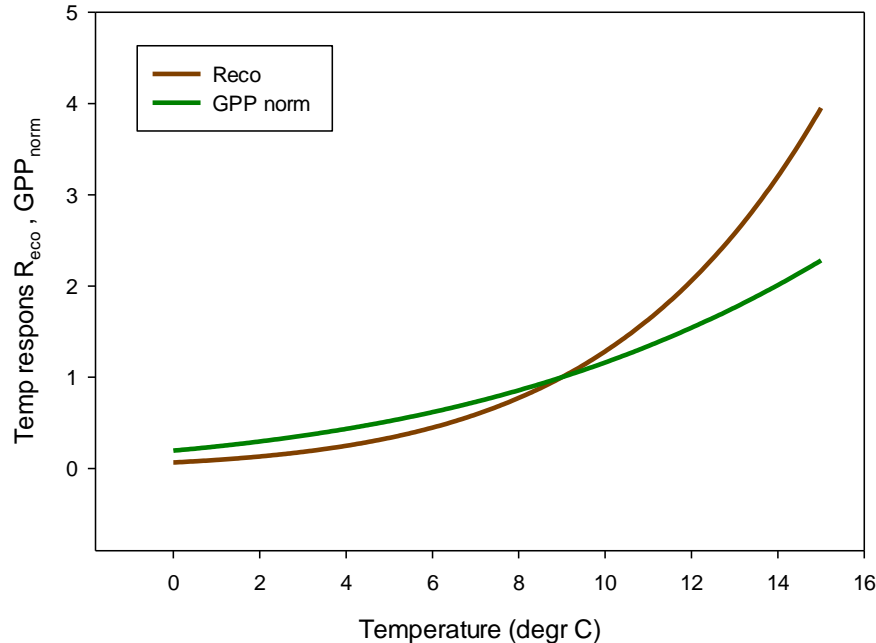


Figure 11. Temperature sensitivity for ecosystem respiration (R_{eco}) (brown) and R_{g} -normalized (positive) gross primary productivity (GPP) (green).

In Fig. 11 we reversed the sign of the GPP temperature response function to make it more easily comparable with the R_{eco} response model. The temperature sensitivity ($\mu\text{mol m}^{-2}\text{s}^{-1} \text{K}^{-1}$) can be estimated from the slope of these curves and the sensitivity is slightly higher for GPP than for R_{eco} in the interval 0 – 4.5 °C, thereafter the difference is small up to about 6 °C then it began to raise rapidly for R_{eco} . We tested what impact this could have by increasing the measured half-hourly air temperature by 1 °C and found that during the growing season the GPP increased by - 31.9 g C m^{-2} and R_{eco} by 36.4 g C m^{-2} . Thus, a slightly larger increase of R_{eco} as compared to GPP resulting in that the small sink of -2.5 gC m^{-2} turns into a source of 4.5 gC m^{-2} .

4.5 CH_4 exchanges

The CH_4 fluxes from the chamber measurements showed large variation over time (Fig. 12) and across sampling locations (Fig. 13). The mean CH_4 flux of all samples was $0.00051 \pm 0.00024 \mu\text{mol m}^{-2}\text{s}^{-1}$. The uncertainty is given as the 95% confidence limit. Setting all fluxes that fell within the flux detection limits to zero changed the mean value with -0.2%. Assuming that the mean flux was representative for the whole of growing season 1, the total CH_4 summer emission was 0.039 to 0.164 $\text{g CH}_4 \text{m}^{-2}$.

We also noticed a clear trend during the summer with highest fluxes in mid-June and then decreasing during the following two sampling occasions. The respective mean values with 95% confidence intervals for the three sampling periods were $0.00121 \pm 0.000512 \mu\text{mol m}^{-2}\text{s}^{-1}$ (June 14-15), $0.000332 \pm 0.000465 \mu\text{mol m}^{-2}\text{s}^{-1}$ (June 26- July 2) and $-0.00000781 \pm 0.0000936 \mu\text{mol m}^{-2}\text{s}^{-1}$ (August 25-26).

473 For CH₄ exchanges we found *ALD*, θ and *GI* to contribute significantly to explain the variance of
 474 the flux (Table 3). The CH₄ flux responded negatively to increasing *ALD* and positively to θ and
 475 *GI*.

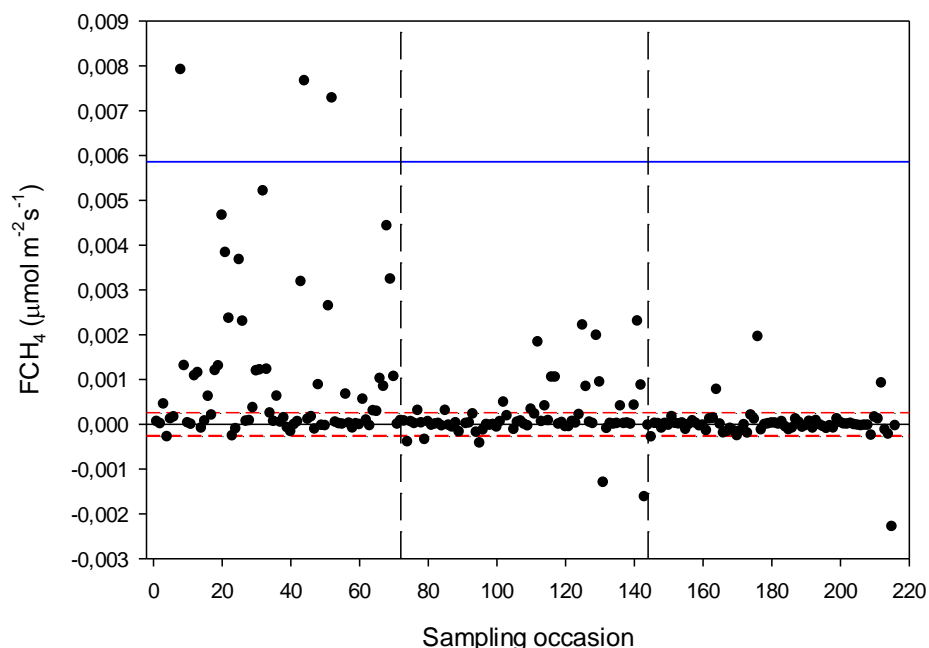
477 Table 3. Result of stepwise multiple linear regression with CH₄ flux as dependent variable.
 478 Normality test failed but significance in all variables was confirmed with Wilcoxon Signed rank
 479 tests. *ALD* is active layer depth, θ is soil moisture and *GI* is green index.

480

Variable	Delta-R ²	Probability (p)
<i>ALD</i>	0.175	<0.001
θ	0.025	0.01
<i>GI</i>	0.020	0.004

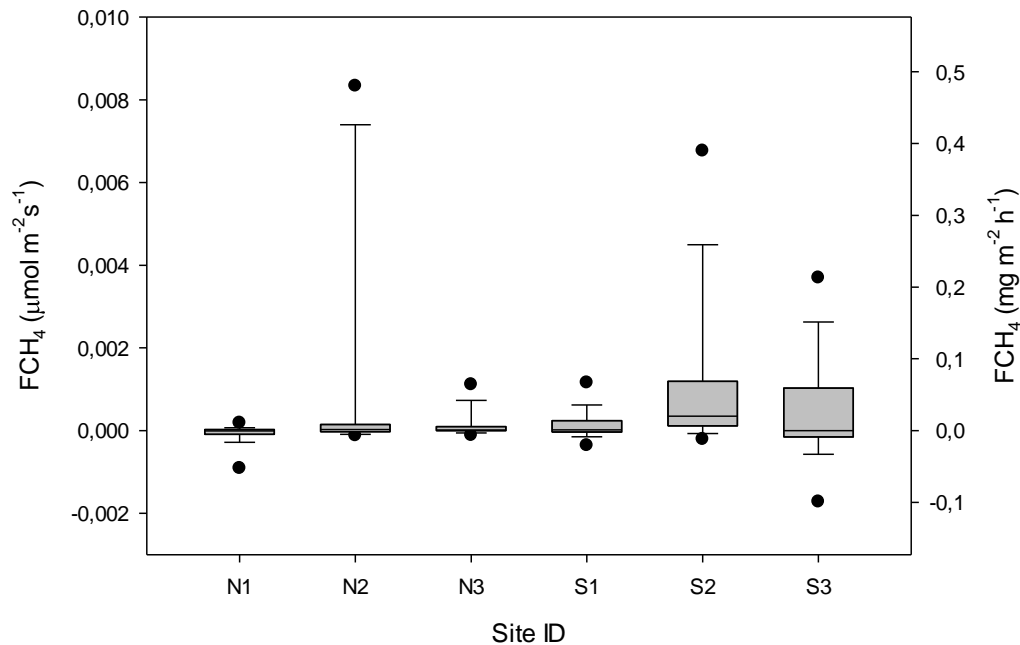
481

482



483

484 Figure 12. Measured CH₄ exchange (FCH₄) from the 24 sampling points using dark chamber and
 485 portable gas analyzer. The dashed red lines indicate CH₄ flux detection limit, (i.e. inside the
 486 limits of detection the exact numbers are highly uncertain) and the blue line represents 3xS.D.
 487 The dashed vertical lines – same as in Fig. 4.



488

489 Figure 13. Box plot of CH₄ fluxes (FCH₄) per sampling location named N1-N3, S1-S3. The
 490 statistics includes also the data that fall within the flux detection limits. The boundaries of the
 491 grey boxes represent the 25% and 75% percentiles, the line represent the median, whiskers above
 492 and below the boxes indicate the 10% and 90% percentiles. Outlying points are also shown.

493 5 Discussion

494 5.1 Seasonal CO₂ fluxes

495

496 We focus our discussion mainly on comparison with other tundra sites located in the North
 497 Atlantic area since these sites are influenced by the North Atlantic Current with its impact on
 498 weather patterns and climate. This limits the comparisons to sites in Greenland, Svalbard and
 499 Northern Scandinavia. However, we broaden the comparison a bit by adding two sites from
 500 Alaska.

501

502 Lund et al. (2012) found that the start of the uptake period was strongly correlated with start of
 503 the snowmelt for the fen in Zackenberg, NE Greenland. They defined the start of snowmelt as
 504 the day when snow depth was <0.1 m. This coincides very well with our definition of start of
 505 growing season (see Fig. 2). Our results for the growing season NEE showing a small net uptake
 506 of -2.5 g C m⁻² is at the low end in comparison with any other high arctic sites which all show a
 507 larger gain of carbon during the growing seasons.

508

509 Lund et al. (2012) analysed 10 years of EC flux measurements from a heathland in Zackenberg
 510 and they reported a NEE range of -39.7 to -4.3 g C m⁻² for the growing season. It was only two
 511 years out of ten that showed NEE values close to zero but still indicating a small net uptake in
 512 Zackenberg heath. Their measured growing season GPP was in the range of -95.4 to -54.1 g C m⁻²
 513 and the R_{eco} was in the range of 37.7 to 63.8 g C m⁻². Our corresponding values were -112.7 g

514 C m⁻² for GPP and 110.2 g C m⁻² for R_{eco}. López-Blanco et al. (2017) presented data over a
515 period of eight years of EC flux measurements from Kobbefjord, SW Greenland over an area of
516 mixed fen and heath vegetation. Their growing season ranges were; for NEE -74.2 to -45.9 g C
517 m⁻², for GPP -316.2 to -181.8 g C m⁻² and for R_{eco} it was 144.2 to 279.2 g C m⁻² excluding 2011
518 which was anomalous because of a pest outbreak and 2014 which did not have a full growing
519 season.

520

521 Our estimate of a small summer NEE of -11.8 g C m⁻² (Table 2) is also different in comparison
522 with other tundra sites which show larger uptake during the summer; for a fen type of vegetation
523 in NE Greenland Soegaard and Nordstroem (1999) reported -96.3 g C m⁻² while Rennermalm et
524 al. (2005) reported -50 g C m⁻² for the same site but for a different year. Groendahl et al. (2007)
525 reported a range of -1.4 to -18.9 g C m⁻² for heath vegetation also on NE Greenland.

526

527 It is difficult to compare growing season values firstly because they are rarely defined the same
528 way. Only small differences in definition of start and end of growing season can have a large
529 impact on the NEE values since NEE is the sum of two large components of almost equal size
530 and of different sign. Secondly, it is also difficult to compare GPP and R_{eco} for any season since
531 the methods to split NEE into components differ from case to case. The most reliable comparison
532 is probably for summer season (June – August) since most studies represents this period best in
533 terms of measurement coverage and quality. And thirdly, there are differences in vegetation type
534 that can have a big impact on gas exchanges. Our moist moss tundra is dominated by moss
535 species and mosses are not as efficient primary producers as vascular plants and this make the
536 net uptake of carbon dioxide small as compared to heath or wet fen systems.

537

538 The climate warming is predicted to be most evident at high latitudes such as the Arctic region.
539 Svalbard has experienced significant warming during the last decades (1971-2017) with 3- 5
540 degrees with the largest increase in the winter and smallest in the summer (Hanssen-Bauer et al.,
541 2019). Our air temperature observations in 2015 are in line with these results (Fig.1). An
542 interesting question is if such changes in temperature has also affected the net carbon balance of
543 the ecosystem? Our analysis of temperature sensitivity of R_{eco} and GPP shows that this could be
544 the case for this site since R_{eco} is increasing more than GPP for temperatures above about 6 °C
545 which occurs quite frequent during the summer (see Fig. 2). Our analyses of the impact of a
546 temperature increase of 1 °C showed that our small sink of -2.5 g C m⁻² during growing season
547 would be turned into a similarly small source of 4.5 g C m⁻² for a 1 degree increase in air
548 temperature. These results are in line of those of Welker et al. (2004) who performed a warming
549 experiment in high Arctic tundra ecosystems. They showed that the net ecosystem exchange in
550 the wet tundra ecosystem decreased by 20% during growing season under a 2 degree warming
551 treatment. This was in contrast to the dry and mesic ecosystems which increased their net carbon
552 uptake by 12-30%.

553

554

555 5.2 CH₄ fluxes

556

557 Our estimated growing season CH₄ flux of 0.08 g C m⁻² is very low compared to most other
558 methane emitting tundra sites; the Zackenberg fen site emitted CH₄ in the range 1.4 to 4.9 g C m⁻²
559 (Mastepanov et al. (2013), Jackowicz-Korczynski et al. (2010) and Jammet et al. (2015)

560 reported 20.1 to 25.1 g CH₄ m⁻² for the Stordalen mire in Northern Sweden. For three different
561 sites in northern Alaska, Bao et al. (2021) reported annual emissions between 1.8 and 8.5 g CH₄
562 m⁻² which corresponds to 0.94 and 4.5 g CH₄ m⁻² for the growing season based on their estimate
563 that growing season emissions are 52.6% of the annual emissions. Sachs et al. (2008) measured
564 CH₄ exchanges with EC method in a northern Siberian polygon tundra and found generally low
565 fluxes of about 18.5 mg CH₄ m⁻² day⁻¹ with little variation over the growing season. This rate
566 adds up to 2.3 g CH₄ m⁻² for their four months long growing season.

567
568 It should be pointed out that we did not perform measurements during the shoulder seasons
569 meaning that we probably underestimate the seasonal total. Importance of shoulder seasons was
570 first pointed out by Mastepanov et al. (2008) which discovered a large burst of CH₄ at and after
571 the onset of soil freezing. One interesting observation is that the main part of our CH₄ flux
572 occurred during the sampling period 14-15 June 2016 which is about 30 days after snow melt.
573 This is the time of the season when CH₄ emissions normally are peaking (Mastepanov et al.
574 2013). After that, the rates dropped to practically zero in late August (see Fig. 12).

575
576
577 The comparison between the different sites are hampered by the fact that they in most cases
578 belong to different bioclimatic subzones with differences in climate and vegetation (Walker et
579 al., 2005). The only site besides Kapp Linne that belong to subzone B is the one in Ny Ålesund.
580 The other high Arctic sites Adventdalen and Zackenberg both belong to subzone C, the
581 intermediate high/low Arctic sites Kobbefjord and Disco Island belongs to subzone D
582 respectively C/D. The low Arctic site Atqasuk belong to subzone D and the Imnavait Creek
583 belong to subzone E. The sub-Arctic Abisko is not classified by Walker et al. (2005) but based
584 mean July air temperature it should belong to subzone E. These differences in climate and
585 vegetation should be kept in mind when comparing results from different sites.

586 587 5.3 Environmental controls of fluxes

588
589 A key issue in high Arctic is how ecosystems with soil that contain large amounts of frozen
590 carbon will respond to warming. A recent report about the future climate of Svalbard (Hanssen-
591 Bauer et al. 2019) show that appalling changes are at risk to occur. By 2071-2100 compared to
592 1971-2000 the mean annual temperature is estimated to increase by 7 °C to 10 °C for the medium
593 and high emission scenarios, respectively. Precipitation is also estimated to increase by 45%
594 respectively 65% for these scenarios. Such large changes will of course also have a lot of other
595 impacts as well for instance shorter snow season, more erosion and sediment transport, changes
596 in vegetation composition and growth etc etc. Assessment of such large changes are very
597 difficult and is far beyond the scope of this paper. We have however shown that for a smaller
598 temperature increase of 1 degree, the impact on the net carbon balance during the growing
599 season will be minute; the increase in ecosystem respiration is compensated for by a
600 corresponding, or actually slightly larger increase of gross primary productivity. Similar
601 compensation effect was obtained for a heath site in Zackenberg by Lund et al. (2012). They
602 used multi-year measurements to assess the effect of changes in temperature on the growing
603 season fluxes

604

605 We found that air temperature was the main control of ecosystem respiration followed by soil
606 moisture and greenness index (Table 1). We had expected that soil temperature should contribute
607 significantly to explain the variations in R_{eco} but it did not. Cannone et al. (2019) showed that
608 ground surface temperature at 2 cm depth contributed significantly to explain R_{eco} in nearby
609 Adventdalen during early, peak and late parts of the growing season. In their study soil moisture
610 was also significant during peak and late seasons. One possible explanation to this difference in
611 responses could be that our soil temperature was measured at 5 cm depth and that air temperature
612 was more representative for the microbial processes taking place in or near the soil surface.
613 Interestingly, GI contributed significantly to explain variations in R_{eco} . The GI was clearly
614 correlated with the abundance of *Salix polaris* (see Supplement) and thus we interpret the
615 positive correlation between GI and R_{eco} to be an effect of increasing contribution by autotrophic
616 respiration to the total respiration.

617 We found no significant correlation between CH_4 emission and temperature. The best
618 explanation was by active layer depth followed by soil moisture and GI (Table 3). But it should
619 be pointed out that ALD and θ are not independent from each other and that ALD can be
620 regarded as a proxy for any seasonal variability, like plant phenology. Soil moisture decreases
621 with increasing active layer depth. The correlation between GI and CH_4 emission is probably
622 also connected with abundance of the vascular plant *Salix polaris*. Vascular plants are since long
623 mentioned as a pathway for CH_4 from the soil interior to the atmosphere in wet tundra
624 ecosystems (e.g. Schimel, 1995) but it could also be an effect of mediation of soil by the root
625 exudation of organic acids as mentioned by Ström et al. (2012). However, we have not found any
626 studies supporting the latter hypothesis concerning *Salix polaris*.

627 **6 Conclusions**

628 Our analyses of EC and chamber flux measurements have shown that the moss tundra on Kapp
629 Linne is a small sink of CO_2 and a small source of CH_4 during the growing season. Realizing that
630 the winter season also emit CO_2 , we tentatively conclude that this moist moss tundra is a source
631 on an annual basis. Concerning the magnitude of the CO_2 exchanges during summer we find it to
632 be anomalous compared to fens and heath ecosystems located in the North Atlantic region
633 which all are sinks during the summer. The CH_4 exchange is much lower than for other tundra
634 ecosystems in the region.

635
636 The temperature sensitivity for CO_2 exchange was slightly higher for GPP than for R_{eco} in the
637 low temperature range of 0-4.5 °C, almost similar up to 6 °C and thereafter it was considerably
638 higher for R_{eco} . The consequence of this, for a small increase in air temperature of 1 degree (all
639 other variables assumed unchanged) was that the respiration increased more than photosynthesis
640 turning the small sink into a small source. But a warmer winter period would probably also result
641 in an additionally increased loss of carbon. We cannot rule out that the reason why the moss
642 tundra is close to balance today is an effect of the warming that has already taken place in
643 Svalbard.

644 The analysis of which environmental factors that controlled the small-scale fluxes showed that
645 air temperature dominated for R_{eco} and active layer depth for CH_4 but we also found that
646 greenness index significantly explained part of the variation in these fluxes. For R_{eco} we
647 attributed this to an increased share of autotrophic respiration to the total and for CH_4 we

648 hypothesized that the abundance of the dwarf shrub *Salix polaris* effected the exchange either
649 through internal plant pathway for methane or through increased provision of C substrate to the
650 anaerobic microbial community stimulating the production of methane. This finding is an
651 indication that modeling of CO₂ as well as of CH₄ fluxes can be improved by also considering
652 differences and changes in greenness of the vegetation.

653 **7 Supplement**

654 The supplement contains some additional photographs of equipment, site and color photographs
655 of vegetation within the frames used for chamber measurements.

656 **8 Data availability**

657 Data can be obtained from <https://zenodo.org> ([10.5281/zenodo.5704508](https://zenodo.org/record/10.5281/zenodo.5704508)).

658 **9 Author contribution**

659 AL designed the study and wrote the manuscript. NP and AL performed the EC measurements
660 and analysed the EC data. ISJ did the vegetation characterization. AL, CS, LK and MBN
661 performed the chamber measurements. All authors have read and commented the manuscript.

662 **10 Competing interests**

663 We declare no competing interests.

664 **11 Acknowledgments**

665 This work did not receive any other funding except salaries for the authors from their respective
666 organizations. Observations of air temperature, relative humidity, precipitation, ground ice
667 conditions and snow depth were obtained from Norwegian Centre for Climate Services (NCCS)
668 and provided under licence CC BY 4.0. Global radiation data from Adventdalen was obtained
669 from the University Centre in Svalbard (UNIS). Thanks to associated professor Jonas Åkerman,
670 Lund University for support with information about the site.

671

672 **12 References**

673 Arias, P. A., Bellouin, E., Coppola, R.G. et al.: Technical Summary, in: Climate Change 2021:
674 The Physical Science Basis. Contribution of Working Group I to the Sixth Assessment
675 Report of the Intergovernmental Panel on Climate Change, edited by: Masson-Delmotte,
676 V., P. Zhai, A. Pirani, S. L. Connors, C. Péan, S. Berger, N. Caud, Y. Chen, L. Goldfarb,
677 M. I. Gomis, M. Huang, K. Leitzell, E. Lonnoy, J.B.R. Matthews, T. K. Maycock, T.
678 Waterfield, O. Yelekçi, R. Yu and B. Zhou, Cambridge University Press, In Press, 2021.

679 Bao, T., Xu, X., Jia, G., Billesbach, D.P. and Sullivan, R.C.: Much stronger tundra methane
680 emissions during autumn freeze than spring thaw, *Global Change Biology*, 27, 376–387,
681 [https://doi.org/ 10.1111/gcb.15421](https://doi.org/10.1111/gcb.15421), 2021

682 Bosiö, J., Stiegler, C., Johansson, M., Mbufong, H. N. and Christensen, T. R.: Increased
683 photosynthesis compensates for shorter growing season in subarctic tundra—8 years of

- 684 snow accumulation manipulations, *Climatic Change*, 127, 321–334,
685 <http://doi.org/10.1007/s10584-014-1247-4>, 2014.
- 686 Burba, G. G., McDermitt, D., Grelle, A., Anderson, D.J. and Xu, L.: Addressing the influence of
687 instrument surface heat exchange on the measurements of CO₂ flux from open-path gas
688 analyzers, *Global Change Biology*, 14, 1854–1876, [https://doi.org/10.1111/j.1365-](https://doi.org/10.1111/j.1365-2486.2008.01606.x)
689 [2486.2008.01606.x](https://doi.org/10.1111/j.1365-2486.2008.01606.x), 2008.
- 690 Callaghan, T.V., Björn, L O., Chapin III, F.S., Chernov, Y., Christensen, T.R., Huntley, B., Ims,
691 R., Johansson, M., Jolly Riedlinger, D., Jonasson, S., Matveyeva, N., Oechel, W.,
692 Panikov, N. and Shaver, G.: Arctic tundra and polar desert ecosystems, in: *Arctic Climate*
693 *Impact Assessment*, edited by: ACIA, Cambridge University Press, 243-352, 2005.
- 694 Cannonea, N., Pontib, S., Christiansen, H.H., Christensen, T.R., Pirk, N. and Guglielmin, M.:
695 Effects of active layer seasonal dynamics and plant phenology on CO₂ land atmosphere
696 fluxes at polygonal tundra in the High Arctic, Svalbard, *Catena*, 174, 142-153,
697 <https://doi.org/10.1016/j.catena.2018.11.013>, 2019.
- 698 Christensen, T.R., Johansson, T., Akerman, H.J. and Mastepanov, M.: Thawing sub-arctic
699 permafrost: Effects on vegetation and methane emissions, *Geophysical Research Letters*,
700 31, L04501, <https://doi.org/10.1029/2003GL018680>, 2004.
- 701 Christensen, T.R., Jackowicz-Korzynski, M., Aurela, M., Crill, P., Heliasz, M., Mastepanov, M.
702 and Friborg, T.: Monitoring the Multi-Year Carbon Balance of a Subarctic Palsa Mire
703 with Micrometeorological Techniques, *Ambio*, 41, 207–217,
704 <https://doi.org/10.1007/s13280-012-0302-5>, 2012.
- 705 Dobler, A., Lutz, J., Landgren, O. and Haugen, J. E.: Circulation Specific Precipitation Patterns
706 over Svalbard and Projected Future Changes, *Atmosphere*, 11, 1378;
707 [doi:10.3390/atmos11121378](https://doi.org/10.3390/atmos11121378), 2021.
- 708
- 709 Euskirchen, E. S., Bret-Harte, M. S., Scott, G. J., Edgar, C., and Shaver, G. R.: Seasonal patterns
710 of carbon dioxide and water fluxes in three representative tundra ecosystems in northern
711 Alaska, *Ecosphere*, 3, 1–19, <https://doi.org/10.1890/ES11-00202.1>, 2012.
- 712
- 713 Euskirchen, E.S., Bret-Harte, M.S., Shaver, G.R., Edgar, C.W., and Romanovsky, V.E.: Long-
714 Term Release of Carbon Dioxide from Arctic Tundra Ecosystems in Alaska, *Ecosystems*,
715 20, 960–974, <http://doi.org/10.1007/s10021-016-0085-9>, 2017.
- 716 Friedlingstein, P., Cox, P., Betts, R., Bopp, L., von Bloh, W., Brovkin, V., Cadule, P., Doney, S.,
717 Eby, M., Fung, I., Bala, G., John, J., Jones, C., Joos, F., Kato, T., Kawamiya, M., Knorr,
718 W., Lindsay, K., Matthews, H. D., Raddatz, T., Rayner, P., Reick, C., Roeckner, E.,
719 Schnitzler, K. G., Schnur, R., Strassmann, K., Weaver, A. J., Yoshikawa, C., and Zeng,

720 N.: Climate-carbon cycle feedback analysis: Results from the C4MIP model
721 intercomparison, *J. Climate*, 19, 3337–3353, <https://doi.org/10.1175/JCLI3800.1>, 2006.

722 Friedlingstein, P., O’Sullivan, M., Jones, M.W. et al.: Global carbon budget 2010, *Earth Syst.*
723 *Sci. Data*, 12, 3269–3340, <https://doi.org/10.5194/essd-12-3269-2020>, 2019.

724 Groendahl, L., Friborg, T., and Soegaard, H.: Temperature and snow-melt controls on
725 interannual variability in carbon exchange in the high Arctic, *Theor. Appl. Climatol.*, 88,
726 111–125, <http://doi.org/10.1007/s00704-005-0228-y>, 2007.

727 Hanssen-Bauer, I., Førland, E.J., Hisdal, H., Mayer, S., Sandø, A.B. and Sorteberg, A.: Climate in
728 Svalbard 2100 – a knowledge base for climate adaptation, Norwegian Environment
729 Agency, Report no. 1/2019., 2019.

730 Hugelius, G., Strauss, J., Zubrzycki, S., Haren, J.W., Schuur, E.A.G., Ping, C.-L., Schirmermeister,
731 L., Grosse, G., Michaelson, G.J., Koven, C.D., O’Donnell, J.A., Elberling, B., Mishra,
732 U., Camill, P., Yu, Z., Palmtag, J. and Kuhry, P.: Estimated stocks of circumpolar
733 permafrost carbon with quantified uncertainty ranges and identified data gaps,
734 *Biogeosciences*, 11, 6573–6593, <http://doi.org/10.5194/bg-11-6573-2014>, 2014.

735 Jackowicz-Korczynski, M., Christensen, T. R., Backstrand, K., Crill, P., Friborg, T.,
736 Mastepanov, M. and Strom, L.: Annual cycle of methane emission from a subarctic
737 peatland, *J. Geophys. Res.-Biogeo.*, 115, G02009, <http://doi.org/10.1029/2008JG000913>,
738 2010.

739 Jammet, M., Crill, P., Dengel, S. and Friborg, T.: Large methane emissions from a subarctic
740 lake during spring thaw: Mechanisms and landscape significance. *J. Geophys. Res.-*
741 *Biogeo.*, 120, 2289-2305, <http://doi.org/10.1002/2015JG003137>, 2015.

742 Kljun, N., Calanca, P., Rotach, M.W., and Schmid, H.P.: A simple two-dimensional
743 parameterisation for Flux Footprint Prediction (FFP), *Geosci. Model Dev.*, 8, 3695-3713,
744 <http://doi.org/10.5194/gmd-8-3695-2015>, 2015.

745 Lasslop, G., Reichstein, M., Papale, D., Richardson, A., Arneth, A., Barr, A., Stoy, P. and
746 Wohlfahrt, G.: Separation of net ecosystem exchange into assimilation and respiration
747 using a light response curve approach: critical issues and global evaluation. *Global*
748 *Change Biology*, 16, 187-208, <https://doi.org/10.1111/j.1365-2486.2009.02041.x>, 2010.

749 Li-Cor: EddyPro® Software (Version 6.0), Li-Cor Inc., Lincoln, USA, 2016.

750 Lloyd, J., and Taylor, J.A.: On the temperature dependence of soil respiration, *Functional*
751 *Ecology*, 8(3), 315-323, 1994.

752 Lopez-Blanco, E., Lund, M., Williams, M., Tamstorf, M.P., Westergaard-Nielsen, A., Exbrayat,
753 J.-F., Hansen, B.U., and Christensen, T.R.: Exchange of CO₂ in Arctic tundra: impacts of

- 754 meteorological variations and biological disturbance, *Biogeosciences*, 14, 4467–4483,
755 <https://doi.org/10.5194/bg-14-4467-2017>, 2017.
- 756 Lund, M., Falk, J. M., Friborg, T., Mbufong, H. N., Sigsgaard, C., Soegaard, H., and Tamstorf,
757 M. P.: Trends in CO₂ exchange in a high Arctic tundra heath, 2000–2010, *J. Geophys.*
758 *Res.- Biogeo.*, <https://doi.org/10.1029/2011JG001901>, 2012.
- 759 Lüers, J., Westermann, S., Piel, K., and Boike, J.: Annual CO₂ budget and seasonal CO₂
760 exchange signals at a high Arctic permafrost site on Spitsbergen, Svalbard archipelago,
761 *Biogeosciences*, 11, 6307–6322, <http://doi.org/10.5194/bg-11-6307>, 2014.
- 762 Mastepanov, M., Sigsgaard, C., Dlugokencky, E. J., Houweling, S., Strom L., Tamstorf, M. P.,
763 and Christensen, T. R.: Large tundra methane burst during onset of freezing, *Nature*, 456,
764 628–631, <http://doi.org/10.1038/nature07464>, 2008.
- 765 Mastepanov, M., Sigsgaard, C., Tagesson, T., Ström, L., Tamstorf, M. P., Lund, M., and
766 Christensen, T. R.: Revisiting factors controlling methane emissions from high-Arctic
767 tundra, *Biogeosciences*, 10, 5139–5158, <https://doi.org/10.5194/bg-10-5139-2013>, 2013.
- 768 McGuire, A. D., Christensen, T. R., Hayes, D., Heroult, A., Euskirchen, E., Kimball, J. S.,
769 Koven, C., Lafleur, P., Miller, P. A., Oechel, W., Peylin, P., Williams, M., and Yi, Y.: An
770 assessment of the carbon balance of Arctic tundra: comparisons among observations,
771 process models, and atmospheric inversions, *Biogeosciences*, 9, 3185–3204,
772 <https://doi.org/10.5194/bg-9-3185-2012>, 2012.
- 773 Myers-Smith, I. H., Kerby, J. T., Phoenix, G. K., Bjerke, J. W., Epstein, H. E., Assman, J. J.,
774 John, C., Adreu-Hayles, L., Angers-Blondin, S., Beck, P. S. A., Berner, L. T., Bhatt, U.
775 S., Bjorkman, A. D., Blok, D., Bryn, A., Christiansen, C. T., Cornelissen, J. H. C.,
776 Cunliffe, A. M., Elmendorf, S. C., Forbes, B. C., Goetz, S. J., Hollister, R. D., de Jong,
777 R., Loranty, M. M., Marcias-Fauria, K., Maseyk, K., Normand, S., Olofsson, J., Parker,
778 T. C., Parmentier, F.-J. W., Post, E., Schaepman-Strub, G., Stordal, F., Sullivan, P. F.,
779 Thomas, H. J. D., Tømmervik, H., Treharne, R., Tweedie, C. E., Walker, D. A.,
780 Wilmking, M. and Wipf, S.: Complexity revealed in the greening of the Arctic, *Nat.*
781 *Clim. Chang.*, 10, 106–117, <https://doi.org/10.1038/s41558-019-0688>, 2020.
- 782 Oechel, W. C., C. A. Laskowski, G. Burba, B. Gioli, and Kalhori, A.A.M.: Annual patterns and
783 budget of CO₂ flux in an Arctic tussock tundra ecosystem, *J. Geophys. Res. Biogeo.*,
784 119, 323–339, <http://doi.org/10.1002/2013JG002431>, 2014.
- 785 Pastorello, G., Trotta, C., Canfora, E. et al.: The FLUXNET2015 dataset and the ONEFlux
786 processing pipeline for eddy covariance data, *Sci Data*, 7, 225,
787 <https://doi.org/10.1038/s41597-020-0534-3>, 2020.
- 788 Pirk, N., Sievers, J., Mertes, J., Parmentier, F.-J. W., Mastepanov, M., and Christensen, T. R.:
789 Spatial variability of CO₂ uptake in polygonal tundra: assessing low-frequency

- 790 disturbances in eddy covariance flux estimates, *Biogeosciences*, 14, 3157–3169,
791 <https://doi.org/10.5194/bg-14-3157-2017>, 2017.
- 792 Post, E., Forchhammer, M. C., Bret-Harte, M. S., Callaghan, T. V., Christensen, T. R., Elberling,
793 B., Fox, A. D., Gilg, O., Hik, D. S., Høye, T. T., Ims, R. A., Jeppesen, E., Klein, D. R.,
794 Madsen, J., McGuire, A. D., Rysgaard, S., Schindler, D. E., Stirling, I., Tamstorf, M. P.,
795 Tyler, N. J. C., van der Wal, R., Welker, J., Wookey, P. A., Schmidt, M. and Astrup, P.:
796 Ecological dynamics across the arctic associated with recent climate change, *Science*,
797 325, 1355–1358, <http://doi.org/10.1126/science.1173111>, 2009.
- 798 Ravolainen, V., Soininen, E. M., Jónsdóttir, I. S., Eischeid, I., Forchhammer, M., van der Wal,
799 R. and Pedersen, A. Ø.: High Arctic ecosystem states: Conceptual models of vegetation
800 change to guide long-term monitoring and research, *Ambio*, 49, 666–677,
801 <https://doi.org/10.1007/s13280-019-01310-x>, 2020.
- 802 Rennermalm, A.K., Soegaard, H., and Nordstroem, C.: Interannual Variability in Carbon
803 Dioxide Exchange from a High Arctic Fen Estimated by Measurements and Modeling,
804 *Arctic, Antarctic, and Alpine Research*, 37(4), 545-556, [https://doi.org/10.1657/1523-0430\(2005\)037\[0545:IVICDE\]2.0.CO;2](https://doi.org/10.1657/1523-0430(2005)037[0545:IVICDE]2.0.CO;2), 2005.
- 806 Richardson, A. D., Braswell, B. H., Hollinger, D. Y., Jenkins, J. P. and Ollinger, S. V.: Near-
807 surface remote sensing of spatial and temporal variation in canopy phenology, *Ecological*
808 *Applications*, 19, 1417–1428, <http://doi.org/10.1890/08-2022.1>, 2009.
- 809 Sachs, T., Wille, C., Boike, J., and Kutzbach, L.: Environmental controls on ecosystem-scale
810 CH₄ emission from polygonal tundra in the Lena river delta, Siberia, *J. Geophys. Res.-*
811 *Biogeosci.*, 113, G00A03, <http://doi.org/10.1029/2007JG000505>, 2008.
- 812 Saunio, M., Stavert, A.R., Poulter, B et al.: The global methane budget 2000-2017, *Earth Syst.*
813 *Sci. Data*, 12, 1561–1623, <https://doi.org/10.5194/essd-12-1561>, 2020.
- 814 Schimel, J.P.: Plant Transport and Methane Production as Controls on Methane Flux from Arctic
815 Wet Meadow Tundra, *Biogeochemistry*, 28 (3), 183-200,
816 <https://doi.org/10.1007/BF02186458>, 1995.
- 817 Schuur, E. A. G., McGuire, A. D., Schadel, C., Grosse, G., Harden, J. W., Hayes, D. J.,
818 Hugelius, G., Koven, C. D., Kuhry, P., Lawrence, D. M., Natali, S. M., Olefeldt, D.,
819 Romanovsky, V. E., Schaefer, K., Turetsky, M. R., Treat, C. C., and Vonk, J. E.: Climate
820 change and the permafrost carbon feedback, *Nature*, 520, 171–179,
821 <https://doi.org/10.1038/nature14338>, 2015.
- 822 Soegaard, H. & Nordstroem, C.: Carbon dioxide exchange in a high-arctic fen estimated by eddy
823 covariance measurements and modeling, *Glob. Change Biol.*, 5, 547–562,
824 <https://doi.org/10.1111/j.1365-2486.1999.00250.x>, 1999.

- 825 Strom, L., Tagesson, T., Mastepanov, M., and Christensen, T. R.: Presence of *Eriophorum*
826 *scheuchzeri* enhances substrate availability and methane emission in an Arctic wetland,
827 *Soil Biol. Biochem.*, 45, 61–70, <http://doi.org/10.1016/j.soilbio.2011.09.005>, 2012.
828
- 829 Walker, D. A., Raynolds, M. K., Daniëls, F. J. A., Einarsson, E., Elvebakk, A., Gould, W. A.,
830 Katenin, A. E., Kholod, S. S., Markon, C. J., Melnikov, E. S., Moskalenko, N. G., Talbot,
831 S. S., Yurtsev, B. A. and the other members of the CAVM Team: The Circumpolar
832 Arctic vegetation map, *Journal of Vegetation Science*, 16, 267-282,
833 <https://doi.org/10.1111/j.1654-1103.2005.tb02365.x>, 2005.
- 834 Welker, J.M., Fahnestock, J.T., Henry, G.H.R., O’Dea, K.W. and Chimner, R.A.: CO₂ exchange
835 in three Canadian High Arctic ecosystems: response to long-term experimental warming.
836 *Global Change Biology*, 10, 1981-1995. Doi: 1011/j.1365-2486.2004.00857.x, 2004.
837
- 838 Vanderpuye, A. W., Elvebakk, A. and Nilsen, L.: Plant communities along environmental
839 gradients of high-arctic mires in Sassendalen, Svalbard, *J. Veg. Sci.*, 13, 875–884,
840 <http://doi.org/10.1111/j.1654-1103.2002.tb02117.x>, 2002.
841
- 842 Vickers, H., Karlsen, S. R. and Malnes, E.: A 20-Year MODIS-Based Snow Cover Dataset for
843 Svalbard and Its Link to Phenological Timing and Sea Ice Variability, *Remote Sens.*, 12,
844 1123; doi:10.3390/rs12071123, 2020.
845
846
- 847 Wutzler, T., Lucas-Moffat, A., Migliavacca, M., Knauer, J., Sickel, K., Šigut, L., Menzer, O. and
848 Reichstein, M.: Basic and extensible post-processing of eddy covariance flux data with
849 REddyProc, *Biogeosciences*, 15(16), 5015-5030, Doi:10.5194/bg-15-5015-2018, 2018.
- 850 Zhang, W., Jansson, P-E., Sigsgaard, C., McConnella, A., Jammet, M.M., Westergaard-Nielsen,
851 A., Lund, M., Friberg, T., Michelsen, A., and Elberling, B.: Model-data fusion to assess
852 year-round CO₂ fluxes for an arctic heath ecosystem in West Greenland (69°N),
853 *Agricultural and Forest Meteorology*, 272-273, 176-186,
854 <https://doi.org/10.1016/j.agrformet.2019.02.021>, 2019.